Materials and Design 197 (2021) 109270

Contents lists available at ScienceDirect

Materials and Design

journal homepage: www.elsevier.com/locate/matdes

Enhanced energy storage properties of thermostable sandwich-structured $BaTiO_3$/polyimide nanocomposites with better controlled interfaces

Jiasheng Ru [a,b], Daomin Min [a], Michael Lanagan [b,*], Shengtao Li [a,*], George Chen [a]

[a] State Key Laboratory of Electrical Insulation and Power Equipment, School of Electrical Engineering, Xi'an Jiaotong University, Xi'an, Shaanxi 710049, PR China
[b] Materials Research Institute, The Pennsylvania State University, University Park, PA 16802, USA

HIGHLIGHTS

- A novel fabrication method was adopted to better control the interfaces of sandwich-structured polyimide nanocomposites.
- A maximum energy density of 5.1 J/cm^3 is reached, while keeping a high thermal stability (3.9 J/cm^3 at 100 °C).
- A model was proposed to understand the effect mechanism of sandwich structure and novel fabrication on breakdown property.

GRAPHICAL ABSTRACT

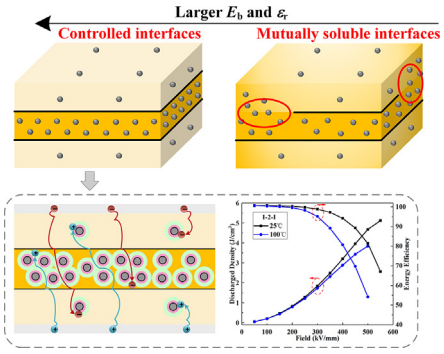

ARTICLE INFO

Article history:
Received 1 September 2020
Received in revised form 25 October 2020
Accepted 25 October 2020
Available online 28 October 2020

Keywords:
Sandwich structure
Polyimide nanocomposites
Energy storage
Energy density
Interface
Breakdown mechanism

ABSTRACT

The energy density of polymers for high temperature applications is still relatively low. Among them, polyimide (PI) is one of the most attractive matrixes because of its high thermal stability. Instead of the mono thermal imidization method to fabricate multilayer PI nanocomposites in the literature, a novel method was proposed herein to better control the multilayer morphology, which could help to further enhance the energy storage properties. The method's effect on the morphology especially on the interfaces between adjacent layers was studied, and then the mechanism of breakdown strength change was discussed by a proposed model based on bipolar charge transport. The sandwich-structured PI nanocomposites, composed of the middle polarization layer with high $BaTiO_3$ (BT) content and the two outer insulation layers with low BT content, were fabricated. Enhanced breakdown field and discharged energy density of 550 kV/mm and 5.1 J/cm^3 with the efficiency of about 70% were achieved, while keeping a high thermal stability (500 kV/mm and 3.9 J/cm^3 at 100 °C). This work presents a promising polymer nanocomposite for energy storage capacitors especially in extreme temperature environments, and a new concept to fabricate multilayer dielectric composites.

1. Introduction

Advanced electrical energy storage devices are quite imperative for the development of modern electronics and power systems. Comparing to other energy storage devices, polymer film capacitors possess the advantages of large power density, high operating voltage, excellent mechanical flexibility and unique self-healing ability. They are promising in many applications [1,2] such as hybrid electric vehicles, pulsed power sources, and power regulations in smart grid. However, despite the rather high breakdown field E_b of polymer films, their ultimate discharged energy density U_e is limited by the low relative permittivity

* Corresponding authors.
E-mail addresses: mxl46@psu.edu (M. Lanagan), sli@mail.xjtu.edu.cn (S. Li).

https://doi.org/10.1016/j.matdes.2020.109270

ε_r (usually <3) [2,3]. To meet the urgent demands for compact, low-cost and high-performance capacitors [1], polymer films with high energy density must be developed.

Polymer composites containing ceramic [4,5] or conductive [6–8] nanofillers, and three-phase polymer nanocomposites [9–11] have received extensive attentions, and are expected to increase ε_r through the additional nanofillers while maintaining the high E_b of polymer matrixes. However, the increased ε_r is always obtained at the expense of dramatically decreased E_b, thus failing to enhance U_e significantly. In view of the problem, some effective methods to enhance energy storage performance have been proposed, such as the morphology control and surface functionalization of nanofillers. It was found that the size of nanoparticles [12] and the aspect ratio of one-dimensional (1D) nanofillers [13,14] have a significant impact on the dielectric property of the nanocomposites. Some designed filler structures (shaped fillers [15], superstructures [16,17], networks [18,19], etc.) were also constructed to further enhance the properties. Surface modified nanofillers by coupling agent [20–22] was employed to improve their compatibility with polymer matrixes, while core-shell nanofillers (core-single-shell [23,24], core-double-shell [25,26], core-satellite [27,28], etc.) were introduced into polymer matrixes to mitigate the local field distortion induced by the permittivity contrast between fillers and matrixes.

There are many researchers interested in the spatial orientation and arrangement of nanofillers, which could improve the ε_r and E_b of the composites simultaneously. Aligned 1D nanofillers may lengthen the carrier's migration path in the bulk, which is beneficial for improving E_b. The alignment of 1D nanofillers has been achieved by electrospinning method [29–31], hot stretch-pressing method [32,33], nanowire array method [34,35] and so on, however, it is still difficult to develop a universal and precise alignment technology. The controlled arrangement of nanofillers could be performed by multilayer [36,37], interlayer [38], gradient structure [39], sandwich structure [40–44] and so on, among which sandwich structure has been much more studied. The structure is usually comprised of the polarization layer with larger ε_r and the insulation layer with higher E_b. Ultrahigh U_e ~ 20 J/cm^3 has been achieved in lab-scale capacitors based on several sandwich-structured fluoropolymer nanocomposites.

Owing to its superior mechanical performance, excellent electrical properties, as well as high thermal and chemical stability, polyimide (PI) is one of the most promising polymer films for energy storage capacitors, especially at high temperatures [45–48]. In previous studies, various nanofillers and technologies were introduced into sandwich-structured PI composites, such as amino-modified multi-wall carbon nanotubes (NH_2-MWNTs) [40], $BaTiO_3$ (BT) nanoparticles [42], 0.5Ba$(Zr_{0.2}Ti_{0.8})O_3$–0.5$(Ba_{0.7}Ca_{0.3})TiO_3$ (BZT-BCT) nanofibers and hexagonal boron nitride (h-BN) nanosheets [45], $KTa_{0.5}Nb_{0.5}O_3$ (KTN) nanoparticles [47], SiO_2@$Ba_{0.85}Ca_{0.15}Zr_{0.1}Ti_{0.9}O_3$ (SiO_2@BCZT) nanofibers and hydroxylated h-BN nanosheets [49], BZT-BCT@Fe_3O_4 nanofibers [50]. However, their U_e (1.5–3.3 J/cm^3) are still not high enough.

Instead of the mono thermal imidization (mono-TIM) method to fabricate multilayer PI nanocomposites in the above literature, a novel multi-TIM method, which TIM process was performed layer by layer but not only once, was proposed in the present work. The process difference has a large impact on the multilayer morphology especially on the

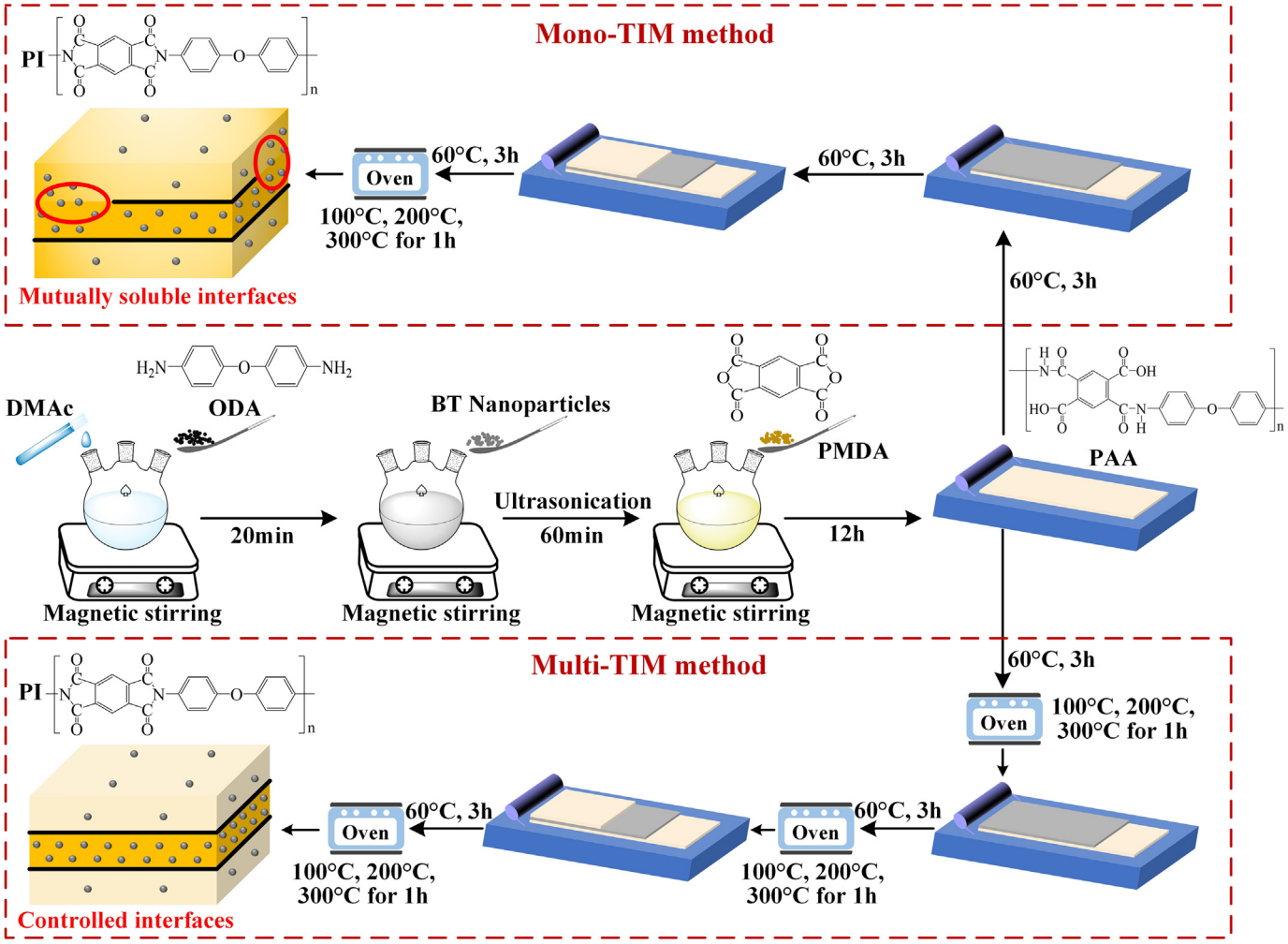

Fig. 1. Schematics of sandwich-structured BT/PI nanocomposites via the two fabrication methods.

interfaces between adjacent layers, and thus change the energy storage properties. Moreover, for the fabrication of sandwich-structured BT/PI nanocomposites, the arrangement of the BT nanoparticles was optimally designed as follows. (i) According to our previous research [51], 0.05 wt% BT/PI possesses the highest E_b, which was employed as the insulation layer; PI nanocomposites with BT content less than 5 wt% (1.2 vol%) couldn't improve the ε_r but dramatically depress the E_b, so only higher BT contents (2–8 vol%) were introduced into the polarization layer. (ii) The polarization layer was selected as the middle layer while the insulation layers were selected as two outer layers. Obviously enhanced E_b and U_e (550 kV/mm and 5.1 J/cm^3) are presented in this work, with the efficiency of about 70%. Among reported sandwich-structured PI nanocomposites, the value should be one of the highest energy densities. This work also provides a new concept to fabricate multilayer dielectric composites.

2. Experimental

2.1. Materials

Bis(4-aminophenyl) ether (ODA) and *N*,*N*-Dimethylacetamide (DMAc) were purchased from Alfa Aesar (USA). Pyromellitic dianhydride (PMDA) was purchased from Sinopharm Chemical Reagent Co., Ltd. (China). BT nanoparticles from Beijing DK Nano Technology Co., Ltd. (China) were used, with the diameter of about 30–60 nm and the true density of 5.85 g/cm^3.

2.2. Sample fabrication

The single-layered BT/PI nanocomposite films were fabricated through in-situ polymerization, solution casting and TIM process. First, ODA was stirred in DMAc for a few minutes until after the complete dissolution of ODA. Second, a target quantity of BT nanoparticles was added into the solution and dispersed by vigorous ultrasonication for 60 min. Third, PMDA was added into the suspension in three portions, and BT/polyamic acid (PAA) mixture was obtained after intense stirring for 12 h. Then, the prepared BT/PAA mixture was cast into wet films on flat glass plates. Finally, the solvent removal (60 °C for 3 h) and the TIM (100 °C, 200 °C, 300 °C for 1 h respectively) were carried out in sequence with a vacuum oven. The density of single-layered PI is about 1.42 g/cm^3.

To fabricate the sandwich-structured BT/PI nanocomposite films, the bottom layer was cast on flat glass plates, while the middle and upper layers were respectively cast on their preceding layers. During the process, mono- or multi-TIM method was employed, as shown in Fig. 1. In this work, the samples via the two methods are respectively abbreviated as "1 T/I-*x*-I" and "3 T/I-*x*-I" (*x* vol% BT in the polarization layer). For the former method, which was employed in previous studies [40,42,45,47,49,50], only solvent removal was performed after every casting, and TIM was not performed until the casting completion of all the three layers. For the latter method, both solvent removal and TIM were performed after every casting. The thickness of each layer in the sandwich-structured films is about 4 μm, which was controlled by the height of the scraper.

2.3. Characterization

The Fourier transform infrared (FTIR) spectra, the crystal structures, and the thermogravimetric analysis (TGA) of the samples were respectively carried out on a spectrometer (Nicolet iS50, Thermo Fisher Scientific), an X-ray diffraction (XRD) meter (D8 Advance, Bruker), and a thermogravimetric analyzer (TGA/DSC3+, Mettler Toledo). The cross-sectional morphology of the nanocomposites was observed by a

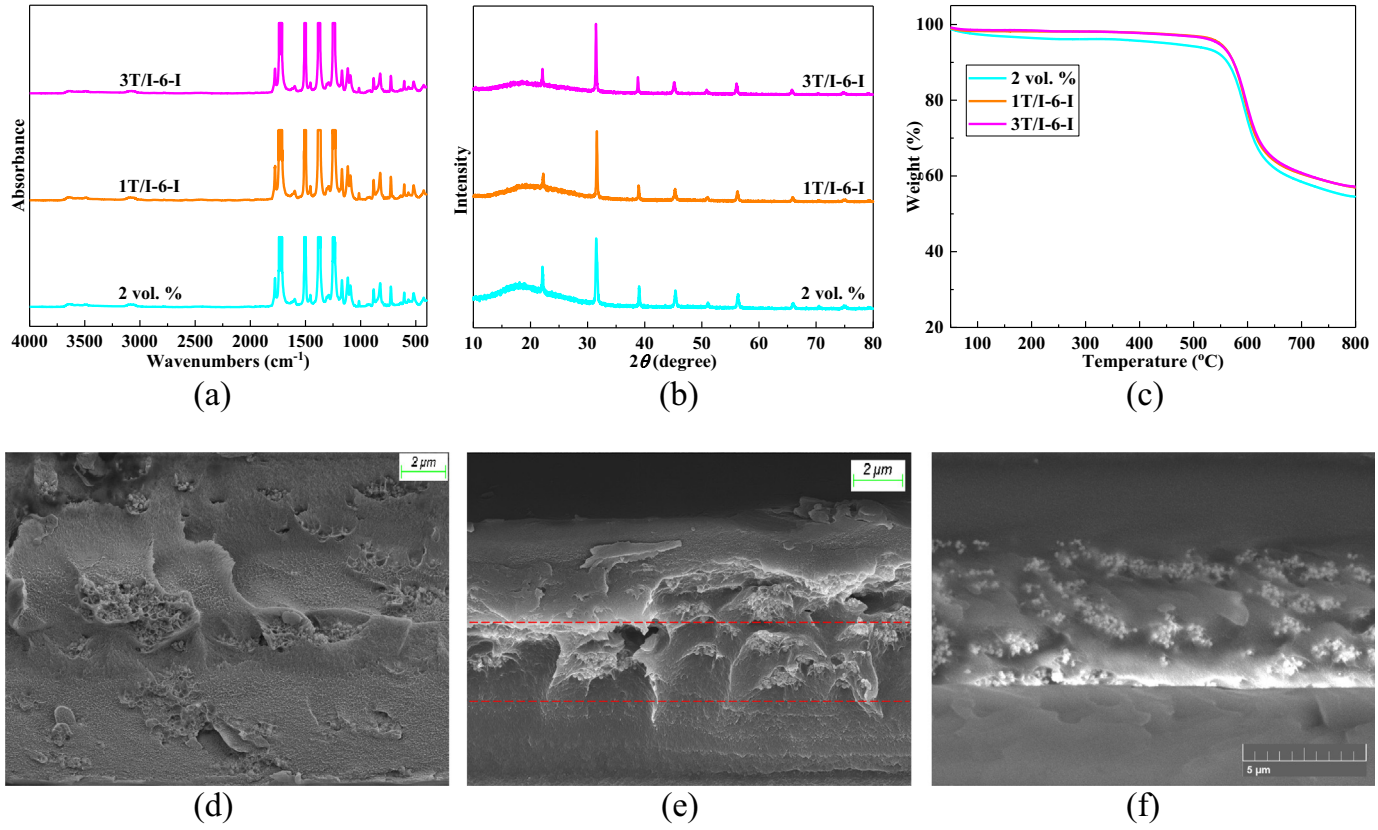

Fig. 2. (a) FTIR spectra, (b) XRD patterns and (c) TGA curves of single-layered 2 vol% BT/PI, 1 T/I-6-I and 3 T/I-6-I films. Cross-sectional SEM images of (d) single-layered 2 vol% BT/PI, (e) 1 T/I-6-I and (f) 3 T/I-6-I films.

scanning electron microscope (SEM, GeminiSEM 500, Zeiss). Samples subjected to the electrical measurements, were coated with concentric gold electrodes by sputtering, with a high voltage electrode of 3 mm diameter and a grounding electrode of 5 mm diameter. The dielectric properties were measured on an impedance analyzer (4294A, Agilent) at room temperature, while using another one (concept 40, Novocontrol) at elevated temperatures. The dc breakdown measurements were performed in a bath containing dielectric fluid (Galden HT-200, Solvay Solexis), with a voltage ramp of 0.5 kV/s. The unipolar *D-E* loops were measured at 100 Hz on an in-house developed apparatus.

3. Results and discussion

To study the effect of the sandwich structure and the two fabrication methods on electrical properties and their mechanisms, a group of samples with essentially the same total BT content, composed of

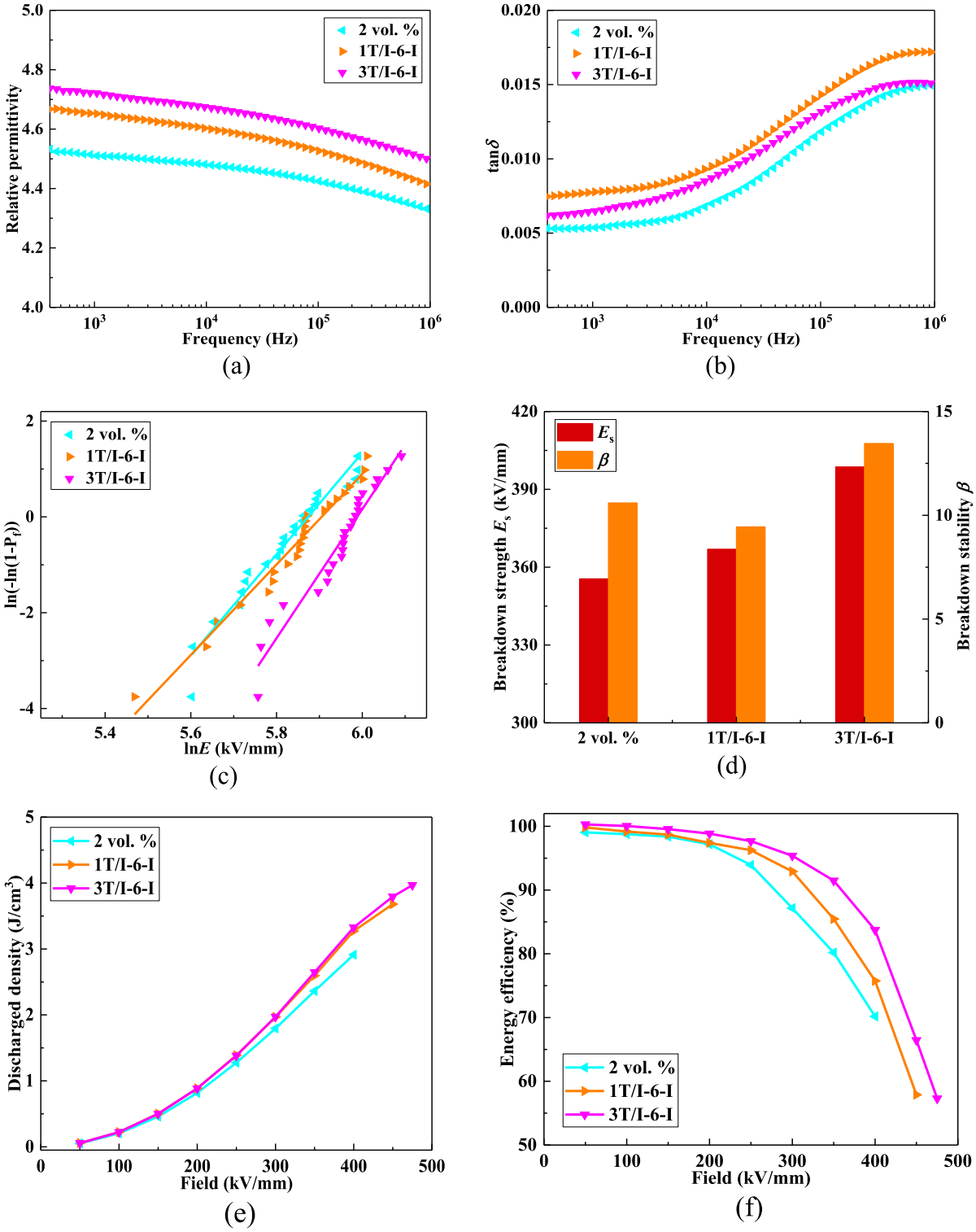

Fig. 3. (a) Relative permittivity, (b) dielectric loss, (c) Weibull breakdown distribution, (d) scale and shape parameters, (e) discharged energy density, (f) energy efficiency of single-layered 2 vol% BT/PI, 1 T/I-6-I and 3 T/I-6-I films.

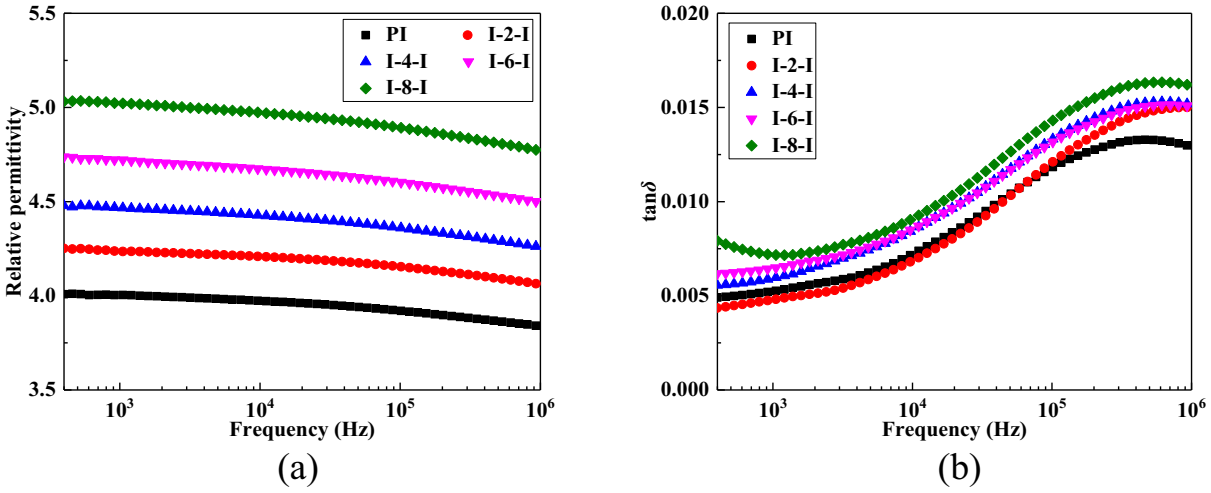

Fig. 4. Frequency-dependent (a) Relative permittivity, and (b) dielectric loss of pure PI and sandwich-structured BT/PI nanocomposites via multi-TIM method.

single-layered 2 vol% BT/PI, 1 T/I-6-I and 3 T/I-6-I films, were studied and compared.

Fig. 2 exhibits the FTIR spectra, XRD patterns, TGA curves and morphology structures of the samples (See Figs. S1-S3 for those of the other samples). In Fig. 2(a), PI-featured absorption peaks (asymmetric C═O stretching at 1780 cm^{-1}, symmetric C═O stretching at 1720 cm^{-1}, C—N stretching at 1380 cm^{-1}, and C═O deformation at 725 cm^{-1}) could be clearly observed in all curves, while PAA-featured peaks (such as –COOH and $-NH_2$ at 2900–3200 cm^{-1}) are not found. The results indicate the accomplishment of imidization. In Fig. 2(b), the broad peak of PI (2θ centered at 18°) and the characteristic peaks of cubic BT could be easily found, which demonstrate the well physical mixture in the nanocomposites. The samples have ultrahigh thermal stability and just start to lose weight when the temperature is increased to about 550 °C, as shown in Fig. 2(c).

In Fig. 2(e) and 2(f), More controllable nanoparticles arrangement, higher interface integrity and better bulk compactness could be observed in the 3 T/I-6-I film. To explain that, several reasonable causes were discussed here. (i) In the mono-TIM method, part of the preceding dried layer may dissolve into the following undried layer especially if the BT content is comparatively high in the dried layer; The mutual dissolution of the middle polarization layer and upper insulation layer could be clearly observed in Fig. 2(e); The phenomenon compromises the integrity of the interfaces between adjacent layers and the designed arrangement of nanoparticles. (ii) Although BT/PAA layers have been totally dried into rigid films, there are still some residual solvents (~20%) [52], moreover, water molecules are produced during the cyclodehydration of PAA; During the preparation of the 1 T/I-6-I film, the residual solvents and water molecules in bottom and central layers are much more difficult to evaporate because of the hindering of upper layer; The phenomenon compromises the compactness of films. These phenomena and their negative effects could be avoided in the multi-TIM method, therefore it should be a more considerable strategy to fabricate multilayer PI composites.

Their electrical properties were also studied. For accuracy, the dc breakdown results were analyzed by a two-parameter cumulative Weibull distribution function

$$P_f(E_s,\beta) = 1 - \exp\left[-\left(\frac{E_m}{E_s}\right)^{\beta}\right] \quad (1)$$

where E_m is the experimental breakdown strength in $kVmm^{-1}$; the scale parameter E_s is the characteristic breakdown strength in $kVmm^{-1}$, and represents the breakdown strength at a cumulative failure

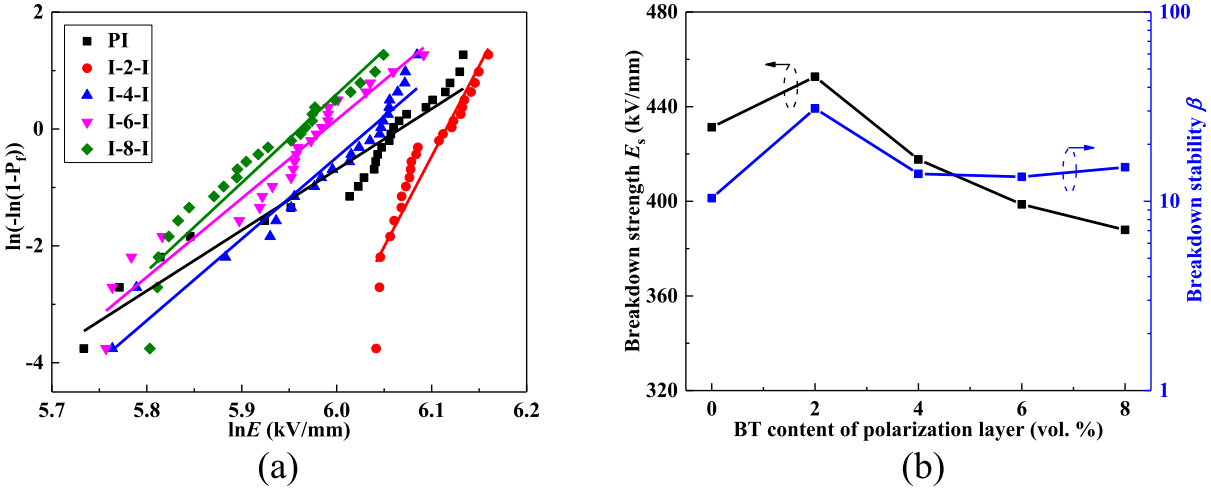

Fig. 5. (a) Weibull breakdown distribution, (b) scale and shape parameters of pure PI and sandwich-structured BT/PI nanocomposites via multi-TIM method.

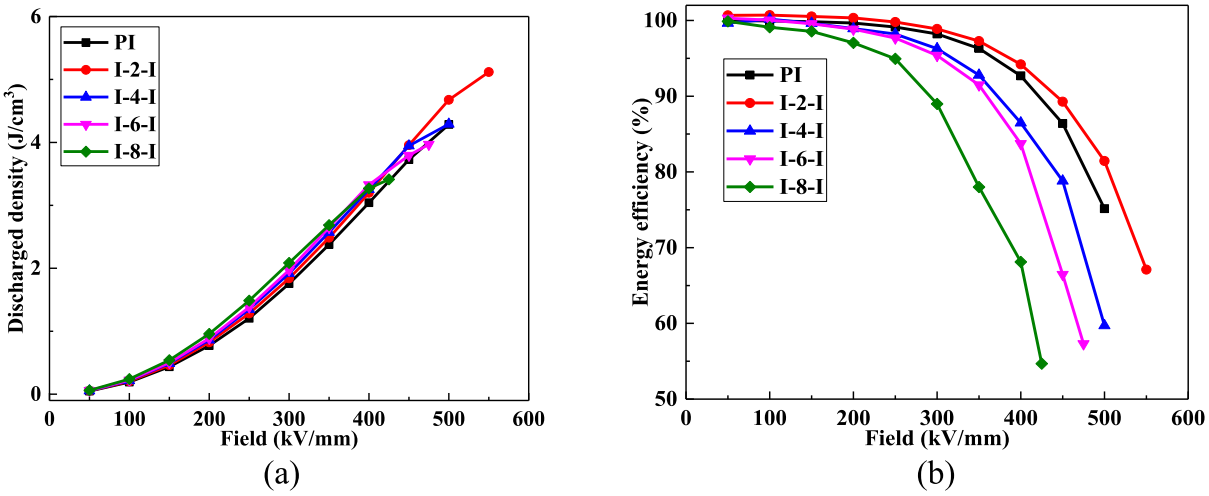

Fig. 6. (a) Discharged energy density and (b) efficiency of pure PI and sandwich-structured BT/PI nanocomposites via multi-TIM method.

probability of 63.2%; the shape parameter β is the breakdown stability, and describes the dispersion of experimental results. To calculate the discharged energy density U and the energy efficiency η, D-E loops under various electric fields were analyzed by Eq. (2) below:

$$U = \int_{D_r}^{D_m} E\mathrm{d}D, \eta = \frac{\int_{D_r}^{D_m} E\mathrm{d}D}{\int_{0}^{D_m} E\mathrm{d}D} \tag{2}$$

where E is the electric field in Vm^{-1}, $D = \varepsilon_0\varepsilon_r E$ is the induced electric displacement in Cm^{-2} (ε_0 is the vacuum permittivity in Fm^{-1}), D_r is the remanent displacement in Cm^{-2}, D_m is the ultimate displacement under an applied electric field in Cm^{-2}.

In comparison with the single-layered film, the two sandwich-structured films possess larger ε_r, higher E_s, and thus enhanced U_e as well as η, as shown in Fig. 3. The ε_r enhancement should be attributed to the interface polarization between adjacent layers and the concentrated distribution of nanoparticles in the polarization layer. Meanwhile, the E_s enhancement should be associated with the field redistribution among the three layers, and the blockade effect on electrical tree growth induced by the interfaces between adjacent layers. However, due to the dielectric loss come from the interface polarization, larger loss could be found at low frequency for the two sandwich-structure films.

Between the two sandwich-structured films in Fig. 3, better properties were obtained in the 3 T/I-6-I but not 1 T/I-6-I film. As discussed above, the 3 T/I-6-I film exhibits more controllable nanoparticles arrangement, higher interface integrity and better bulk compactness. The more integrated interfaces which could provide larger interface polarization and the more compact bulk which could avoid some voids, are distinctly beneficial for the ε_r enhancement. Analogously, the breakdown difference of the two sandwich-structured films is also induced by their morphology characters, which will be discussed later in this work.

Fig. 4 presents the dielectric properties of sandwich-structured BT/PI nanocomposites via multi-TIM method. Similar frequency-dependent behaviors are presented for all the samples, and their excellent dielectric stability indicates the potential for wide frequency band applications. Compared with the single-layered nanocomposites [51], the ε_r increase of sandwich-structured samples is more significant with the increment of BT content, as shown in Fig. 4(a). For instance, the ε_r of I-8-I is about 5.1, which is close to that of the single-layered sample with 20 wt% BT (~5.8 vol% BT). This is attributed to the interface polarization and the concentrated distribution of nanofillers. In sandwich structure, the interfaces between adjacent layers could store additional charges. Besides, concentrated distribution of nanofillers could provide a benefit to ε_r because of its nonlinear increase with the increment of BT content [12].

In Fig. 4(b), all the samples possess quite low dielectric loss, which are smaller than 0.02 over the frequency range of 10^2–10^6 Hz. Unlike the single-layered nanocomposites, the dielectric loss of sandwich-structured samples at low frequency is not only governed by the conductivity, but also influenced by the interface polarization. This should be the reason for the comparatively low loss of pure PI. Besides, a loss peak could be found at the frequency of about 5×10^5 Hz, which is an intrinsic peak of PI with the calculated activation energy of about 0.37 eV (See Fig. S4 and its discussion). The peak origin should be the coupled water molecules and the limited motions of carbonyl groups.

Fig. 5 shows the Weibull breakdown distribution of sandwich-structured BT/PI nanocomposite films via multi-TIM method. With the increment of BT content, the characteristic breakdown strength E_s

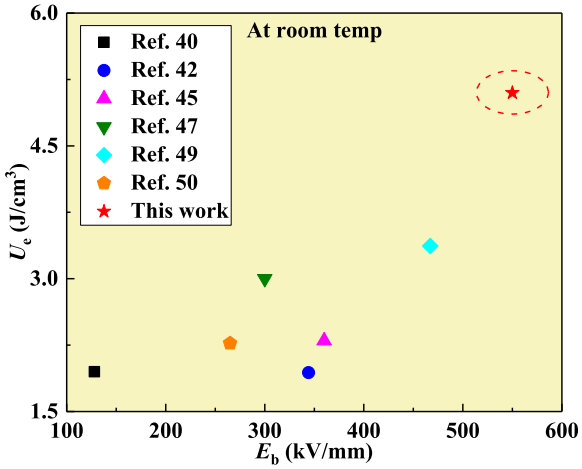

Fig. 7. Comparison in E_b and U_e between this work and the other reported sandwich-structured PI nanocomposites, which include 0–5–0 wt% NH_2-MWNTs [40], 0–3–0 vol% BT nanoparticles [42], 5–1–5 vol% (h-BN nanosheets in two outer layers and BZT-BCT nanofibers in the middle layer) [45], 2–0–2 vol% KTN nanoparticles [47], 1–1–1 vol% (SiO_2@BCZT nanofibers in two outer layers and h-BN nanosheets in the middle layer) [49], 0–5–0 vol% BZT-BCT@Fe_3O_4 nanofibers [50].

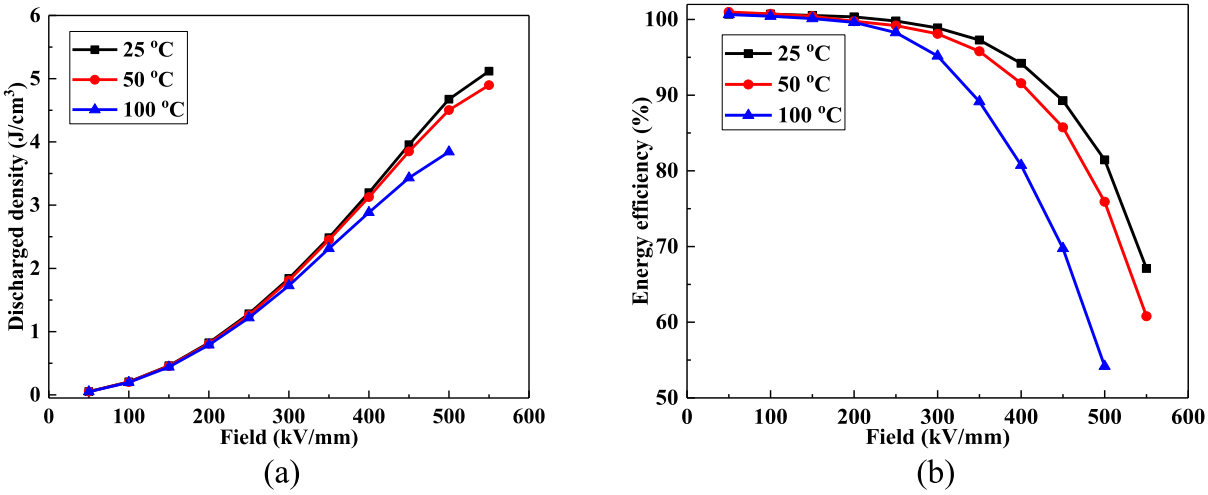

Fig. 8. (a) Discharged energy density and (b) efficiency of 3 T/I-2-I film at elevated temperatures.

decreases after an initial increase, and a maximum value of 453 kV/mm is reached at I-2-I. In comparison with the single-layered nanocomposites [51], the E_s decrease of the sandwich-structured samples is more moderate at high BT content. For instance, the E_s of I-6-I is about 400 kV/mm, which is close to that of the single-layered sample with 5 wt% BT (~1.2 vol% BT). As discussed above, field redistribution and interface blockade in sandwich structure are the two important causes. The field redistribution caused by ε_r difference between the layers could reduce the field strength in polarization layer, thus preventing the failure under high applied voltages. Besides, some researches [43,44] have demonstrated that the interfaces between adjacent layers could block the growth of electrical trees. The weakened charge injection in the sandwich structure should be also a cause of E_s enhancement, which will be discussed later in this work.

Benefiting from the improved ε_r of the sandwich-structured nanocomposites, their discharged energy densities under comparatively low applied field are enhanced, as shown in Fig. 6(a). In addition to the ε_r, their U_e are also governed by the E_b, and the maximum E_b and U_e are obtained at I-2-I which are 550 kV/mm and 5.1 J/cm^3 respectively. It is worth noting that, for all the samples, the increase rate of the discharged energy density is much slower near the E_b, which could be attributed to the much larger D_r. Unlike the D_r induced by domains in ferroelectrics, the D_r herein only appears under high applied field and should be caused by the leakage current. In addition, although the breakdown field E_b and the dc breakdown strength E_s follow a similar trend with the increment of BT content, the values of E_b are higher than corresponding those of E_s due to the much faster voltage rise and much shorter voltage time in *D-E* loop measurements. The energy efficiency η, which could describe the fatness of *D-E* loops and is mainly affected by the polarization loss and conductivity loss, decreases obviously with the increasing field in Fig. 6(b). Quite high η are obtained for all the samples, and they are still above 60% near the E_b. For instance, the η of I-2-I under 550 kV/mm is about 67%.

Fig. 7 shows the comparison in E_b and U_e between this work and the other reported sandwich-structured PI nanocomposites. A significant improvement for E_b and U_e has been achieved herein, which should be attributed to the high E_b of the matrix, the optimally designed sandwich structure, and the novel fabrication method.

Fig. 8 presents the discharged energy density and energy efficiency of the 3 T/I-2-I film at elevated temperatures. With the increasing temperature, the larger polarization loss and conductivity loss cause the larger P_r, the lower E_b and the fatter *D-E* loops, and further causing the decrease of U_e and η. Even so, the values of U_e and η are still relatively high (3.9 J/cm^3 and 54% at 100 °C) compared with the other literature, as shown in Fig. 9. The thermostable energy storage properties of the sample should come from the high thermal stability of its E_b, ε_r and dielectric loss (See Fig. S5), which are respectively 500 kV/mm, 4.1 and 0.0047 at 100 °C. While temperature is even higher, the ε_r and high frequency loss still could be maintained, but the much larger leakage current and rather lower E_b would further depress the U_e and η. More discussion about the energy storage properties of PI nanocomposites at elevated temperatures could be found in Ref. [45, 46, 48].

To further study the mechanism of E_b enhancement induced by sandwich structure and multi-TIM method, interfaces between nanoparticles and polymer matrix in polymer composites must be elucidated first. The interface could be described as a multi-region structure, made up of bonded region and transitional region, which was proposed in the preliminary work [55] and developed herein. The strong connection between nanoparticles and polymer matrix such as covalent, ionic and hydrogen bonds, exists in bonded region, where deep traps are

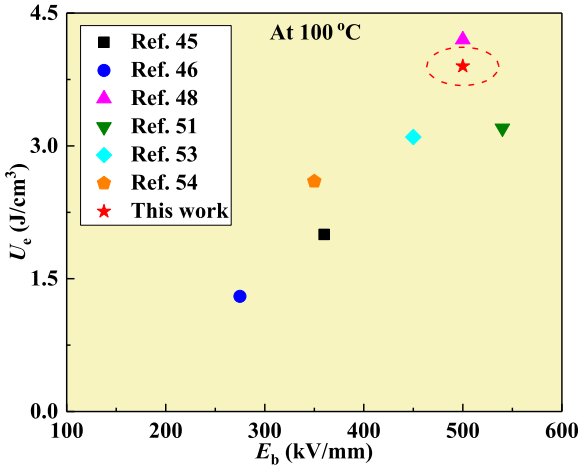

Fig. 9. Comparison in E_b and U_e at 100 °C between this work and the other reported high-temperature polymers, which include 5–1–5 vol% (h-BN nanosheets in two outer layers and BZT-BCT nanofibers in the middle layer) in sandwich-structured PI composite [45], 3 vol% BT nanoparticles in PI composite [46], 1 vol% BT nanofibers in PI composite [48], 0.05 wt% BT nanoparticles in PI composite [51], poly(phthalazinone ether ketone) [53], 0.32 vol% Al_2O_3 nanoparticles in polyetherimide composite [54].

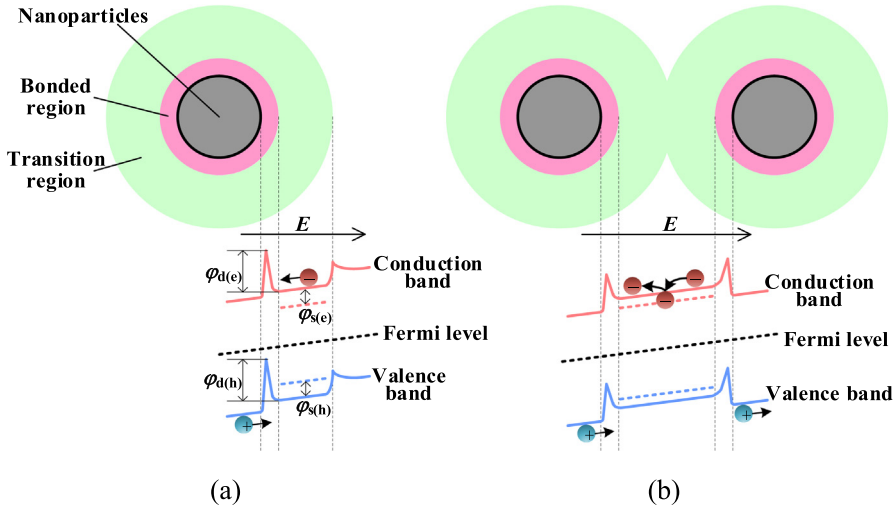

Fig. 10. The schematic of multi-region structure and energy band of the interface between nanoparticles and polymer matrix at (a) low and (b) high content of nanoparticles, where $\varphi_{s(e)}$ and $\varphi_{d(e)}$ are the depths of shallow and deep electron trap in eV; $\varphi_{s(h)}$ and $\varphi_{d(h)}$ are the depths of shallow and deep hole trap in eV.

introduced. In transitional region, polymer chains arrange orderly and are bound by bonded region and nanoparticles; shallow traps are mainly distributed in the region, which could assist the carrier's transport. While the content of nanoparticles is relatively low, the interfaces are almost independent, and thus free electrons and holes are easily captured by the deep traps in bonded region, as shown in Fig. 10(a). At a higher content of nanoparticles, plenty of interfaces are overlapped, and lead to the much larger transitional region and the much smaller trap depth which are beneficial to carrier's detrapping from deep traps, as shown in Fig. 10(b).

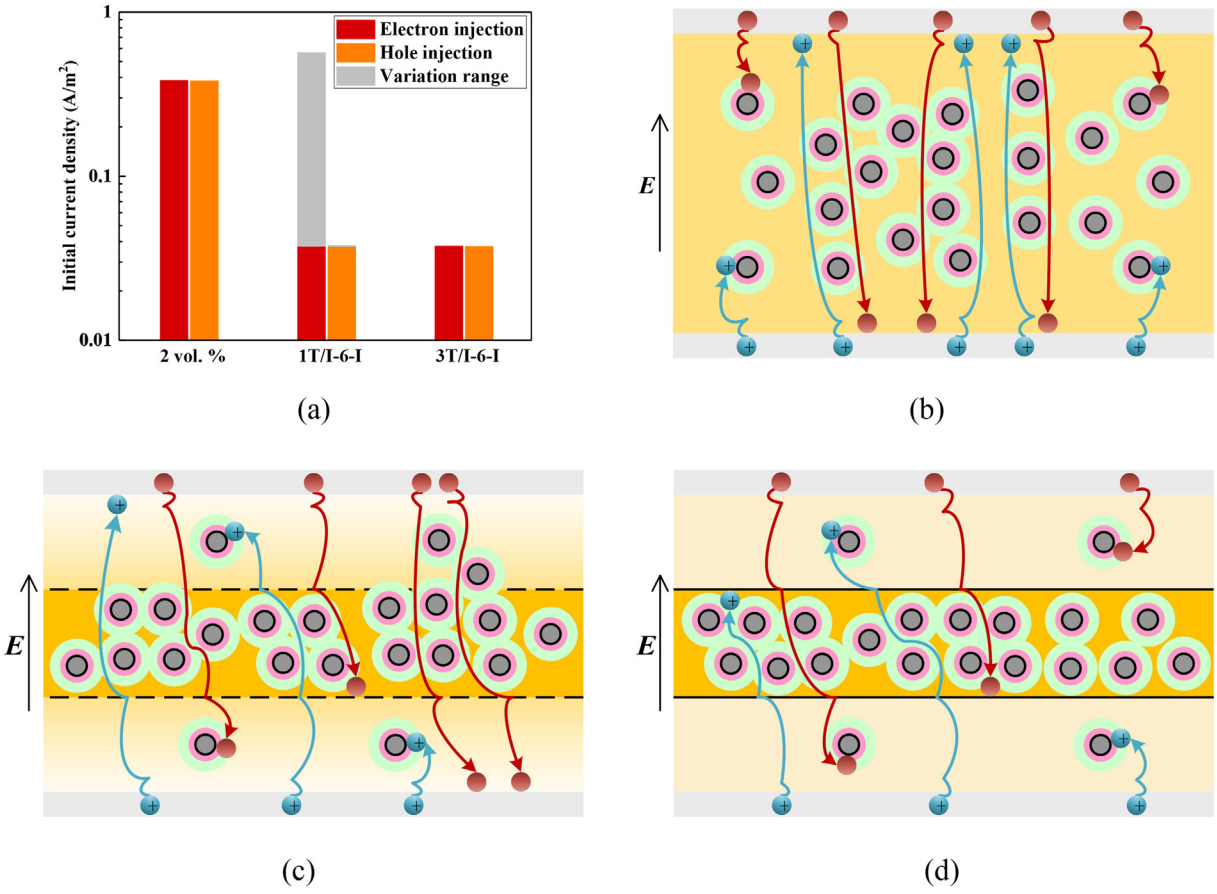

Fig. 11. (a) Initial injection current density of bipolar charge in single-layered 2 vol% BT/PI, 1 T/I-6-I and 3 T/I-6-I films. Proposed mechanism of bipolar charge transport under an applied electric field in (b) single-layered 2 vol% BT/PI, (c) 1 T/I-6-I and (d) 3 T/I-6-I films.

For the polymer nanocomposites under a relatively high field, electrons and holes are injected into the samples by Schottky thermionic emission

$$J_{ei} = AT^2 \exp\left[-\frac{\varphi_{ei}}{k_B T}\right] \exp\left[\frac{\sqrt{\frac{e^3 E_{ei}}{4\pi\varepsilon_0\varepsilon_r}}}{k_B T}\right] \quad (3)$$

$$J_{hi} = AT^2 \exp\left[-\frac{\varphi_{hi}}{k_B T}\right] \exp\left[\frac{\sqrt{\frac{e^3 E_{hi}}{4\pi\varepsilon_0\varepsilon_r}}}{k_B T}\right] \quad (4)$$

where J_{ei} and J_{hi} are the current densities caused by electrons injected from cathode and holes injected from anode, respectively, in Am^{-2}; A is the Richardson constant in $Am^{-2}\,K^{-2}$; T is the temperature in K; φ_{ei} and φ_{hi} are the injection barriers for electrons and holes respectively in eV, which values could be assumed to be the same as the depth of deep traps [56]; k_B is the Boltzmann constant in JK^{-1}; e is the electron charge in C; E_{ei} and E_{hi} are respectively the electric fields at cathode and anode, in Vm^{-1}.

The parameters of single-layered 2 vol% BT/PI, 1 T/I-6-I and 3 T/I-6-I films could be extracted from the curves in Ref. [51], and then their initial injection current densities were calculated and are shown in Fig. 11(a). The initial injection current densities caused by electrons and holes are respectively in the range of 3.74×10^{-2}–5.65×10^{-1} A/m^2 and 3.74×10^{-2}–3.78×10^{-2} A/m^2 for the 1 T/I-6-I film, which values depend on the mutual solubility of the middle and upper layers. According to the discussion of the multi-region structure and the calculation results of injection current, a mechanism model based on bipolar charge transport was proposed, as shown in Fig. 11(b)–11(d).

In the sandwich structure, the outer insulation layers with much deeper traps, which induced by the independent interfaces between nanoparticles and polymer matrix, could effectively hinder the charge injection from electrodes, as shown in Fig. 11(a); moreover, part of free electrons and holes are captured by the deep traps of the insulation layers and the interface barriers between adjacent layers. These effects of the sandwich structure are helpful to maintain a higher E_b than that of the single-layered structure. Between the two sandwich-structured films, the 3 T/I-6-I film possesses more controllable nanoparticles arrangement and integrated interfaces, while part of the middle polarization layer dissolves into the upper insulation layer for the 1 T/I-6-I film. As shown in Fig. 11(c) and 11(d), the disintegrated interfaces would weaken their blockade effect on charge transport in the bulk, and the extra nanoparticles in the upper insulation layer, which evidently change the trap properties, would weaken its hindering effect on charge injection and capture ability of deep traps. As a result, more carrier could pass through the bulk and arrive the opposite electrode for the 1 T/I-6-I film; In other words, breakdown is more possible to occur. Moreover, the worse compactness of the 1 T/I-6-I film also has a negative effect on E_b.

4. Conclusion

Instead of the mono-TIM method to fabricate multilayer PI nanocomposites in the literature, a novel multi-TIM method was proposed herein to further enhance the energy storage properties. The enhancement could be attributed to the more controllable nanoparticles arrangement, higher interface integrity, and better bulk compactness, which effect on the breakdown strength was discussed by a proposed mechanism model based on bipolar charge transport. The sandwich-structured BT/PI nanocomposites, composed of the middle polarization layer with high BT content (2–8 vol%) and the two outer insulation layers with low BT content (0.05 wt%), were fabricated and then studied. Enhanced E_b and U_e are obtained at I-2-I (550 kV/mm and 5.1 J/cm^3 respectively, with the efficiency of about 70%), which should be one of the highest energy densities among reported sandwich-structured PI nanocomposites. More notably, there is a high thermal stability. At 100 °C, the E_b and U_e of I-2-I are 500 kV/mm and 3.9 J/cm^3 respectively, with the efficiency of 54%. This work has shown a promising polymer nanocomposite for energy storage capacitors especially at elevated temperatures, and it also provides a new concept to fabricate multilayer dielectric composites.

Data availability statement

The raw/processed data required to reproduce these findings cannot be shared at this time as the data also forms part of an ongoing study.

CRediT authorship contribution statement

Jiasheng Ru: Conceptualization, Methodology, Validation, Formal analysis, Investigation, Writing - original draft, Writing - review & editing. **Daomin Min:** Validation, Formal analysis, Investigation. **Michael Lanagan:** Conceptualization, Methodology, Funding acquisition, Writing - original draft. **Shengtao Li:** Conceptualization, Methodology, Funding acquisition, Project administration. George Chen: Formal analysis, Investigation.

Declaration of Competing Interest

None.

Acknowledgements

This work was supported by the National Natural Science Foundation of China (Grant No. U1830131). J. Ru gratefully acknowledges the scholarship support from China Scholarship Council (No. 201706280134).

Appendix A. Supplementary data

Supplementary data to this article can be found online at https://doi.org/10.1016/j.matdes.2020.109270.

References

[1] Q. Chen, Y. Shen, S.H. Zhang, Q.M. Zhang, Polymer-based dielectrics with high energy storage density, Annu. Rev. Mater. Res. 45 (2015) 433–458.
[2] H. Luo, X.F. Zhou, C. Ellingford, Y. Zhang, S. Chen, K.C. Zhou, D. Zhang, C.R. Bowen, C.Y. Wan, Interface design for high energy density polymer nanocomposites, Chem. Soc. Rev. 48 (2019) 4424–4465.
[3] V.K. Prateek, R.K. Thakur, Gupta, Recent progress on ferroelectric polymer-based nanocomposites for high energy density capacitors: synthesis, dielectric properties, and future aspects, Chem. Rev. 116 (2016) 4260–4317.
[4] Z.M. Dang, Y.Q. Lin, H.P. Xu, C.Y. Shi, S.T. Li, J.B. Bai, Fabrication and dielectric characterization of advanced $BaTiO_3$/polyimide nanocomposite films with high thermal stability, Adv. Funct. Mater. 18 (2008) 1509–1517.
[5] W. Wan, J.R. Luo, C.E. Huang, J. Yang, Y.B. Feng, W.X. Yuan, Y.J. Ouyang, D.Z. Chen, T. Qiu, Calcium copper titanate/polyurethane composite films with high dielectric constant, low dielectric loss and super flexibility, Ceram. Int. 44 (2018) 5086–5092.
[6] W.H. Xu, Y.C. Ding, S.H. Jiang, J. Zhu, W. Ye, Y.L. Shen, H.Q. Hou, Mechanical flexible PI/MWCNTs nanocomposites with high dielectric permittivity by electrospinning, Eur. Polym. J. 59 (2014) 129–135.
[7] L. Zhang, X. Lu, X.Y. Zhang, L. Jin, Z. Xu, Z.Y. Cheng, All-organic dielectric nanocomposites using conducting polypyrrole nanoclips as filler, Compos. Sci. Technol. 167 (2018) 285–293.
[8] J.W. Shang, Y.H. Zhang, L. Yu, X.L. Luan, B. Shen, Z.L. Zhang, F.Z. Lv, P.K. Chu, Fabrication and enhanced dielectric properties of graphene-polyvinylidene fluoride functional hybrid films with a polyaniline interlayer, J. Mater. Chem. A 1 (2013) 884–890.
[9] J.N. Liu, G.F. Tian, S.L. Qi, Z.P. Wu, D.Z. Wu, Enhanced dielectric permittivity of a flexible three-phase polyimide-graphene-$BaTiO_3$ composite material, Mater. Lett. 124 (2014) 117–119.
[10] J.Y. Kim, T.Y. Kim, J.W. Suk, H. Chou, J.H. Jang, J.H. Lee, I.N. Kholmanov, D. Akinwande, R.S. Ruoff, Enhanced dielectric performance in polymer composite films with carbon nanotube-reduced graphene oxide hybrid filler, Small 10 (2014) 3405–3411.
[11] H.Y. Wang, Q. Fu, J.Q. Luo, D.M. Zhao, L.H. Luo, W.P. Li, Three-phase Fe_3O_4/MWNT/PVDF nanocomposites with high dielectric constant for embedded capacitor, Appl. Phys. Lett. 110 (2017) 242902.

[12] B.H. Fan, J.W. Zha, D.R. Wang, J. Zhao, Z.M. Dang, Experimental study and theoretical prediction of dielectric permittivity in $BaTiO_3$/polyimide nanocomposite films, Appl. Phys. Lett. 100 (2012), 092903, .
[13] H.X. Tang, Z. Zhou, H.A. Sodano, Relationship between $BaTiO_3$ nanowire aspect ratio and the dielectric permittivity of nanocomposites, ACS Appl. Mater. Interfaces 6 (2014) 5450–5455.
[14] N.X. Xu, X.R. Xiao, H. Yang, E.J. Yu, Q.L. Zhang, Enhanced dielectric constant and suppressed dielectric loss of ternary composites based on Ag-P(VDF-HFP) matrix and TiO_2 nanowires, Ceram. Int. 42 (2016) 12475–12481.
[15] W.J. Ji, H. Deng, C. Guo, C.X. Sun, X. Guo, F. Chen, Q. Fu, The effect of filler morphology on the dielectric performance of polyvinylidene fluoride (PVDF) based composites, Compos. Part A 118 (2019) 336–343.
[16] Q.C. Jia, X.Y. Huang, G.Y. Wang, J.C. Diao, P.K. Jiang, MoS_2 nanosheet superstructures based polymer composites for high-dielectric and electrical energy storage applications, J. Phys. Chem. C 120 (2016) 10206–10214.
[17] E.J. Yu, Q.L. Zhang, N.X. Xu, H. Yang, F-TiO_2/P(VDF-HFP) hybrid films with enhanced dielectric permittivity and low dielectric loss, RSC Adv. 7 (2017) 3949–3957.
[18] S.B. Luo, Y.B. Shen, S.H. Yu, Y.J. Wan, W.H. Liao, R. Sun, C.P. Wong, Construction of a 3D-$BaTiO_3$ network leading to significantly enhanced dielectric permittivity and energy storage density of polymer composites, Energy Environ. Sci. 10 (2017) 137–144.
[19] J. Yang, X.T. Zhu, H.L. Wang, X. Wang, C.C. Hao, R.H. Fan, D. Dastan, Z.C. Shi, Achieving excellent dielectric performance in polymer composites with ultralow filler loadings via constructing hollow-structured filler frameworks, Compos. Part A 131 (2020) 105814.
[20] Y.J. Wang, X.J. Wu, C.G. Feng, Q.X. Zeng, Improved dielectric properties of surface modified $BaTiO_3$/polyimide composite films, Microelectron. Eng. 154 (2016) 17–21.
[21] L. Gao, J.L. He, J. Hu, Y. Li, Large enhancement in polarization response and energy storage properties of poly(vinylidene fluoride) by improving the interface effect in nanocomposites, J. Phys. Chem. C 118 (2014) 831–838.
[22] C. Yang, S.J. Hao, S.L. Dai, X.Y. Zhang, Nanocomposites of poly(vinylidene fluoride)-controllable hydroxylated/carboxylated graphene with enhanced dielectric performance for large energy density capacitor, Carbon 117 (2017) 301–312.
[23] Y.N. Hao, Z.P. Feng, Z.D. He, J.M. Zhang, X.M. Liu, J. Qin, L.M. Guo, K. Bi, Gradient design of ultrasmall dielectric nanofillers for PVDF-based high energy-density composite capacitors, Mater. Des. 189 (2020) 108523.
[24] J.C. Wang, Y.C. Long, Y. Sun, X.Q. Zhang, H. Yang, B.P. Lin, Enhanced energy density and thermostability in polyimide nanocomposites containing core-shell structured $BaTiO_3$@SiO_2 nanofibers, Appl. Surf. Sci. 426 (2017) 437–445.
[25] Y.C. Zhou, H. Wang, An Al@Al_2O_3@SiO_2/polyimide composite with multilayer coating structure fillers based on self-passivated aluminum cores, Appl. Phys. Lett. 102 (2013) 132901.
[26] Z.B. Pan, J.W. Zhai, B. Shen, Multilayer hierarchical interfaces with high energy density in polymer nanocomposites composed of $BaTiO_3$@TiO_2@Al_2O_3 nanofibers, J. Mater. Chem. A 5 (2017) 15217–15226.
[27] L.W. Wang, X.Y. Huang, Y.K. Zhu, P.K. Jiang, Enhancing electrical energy storage capability of dielectric polymer nanocomposites via the room temperature Coulomb blockade effect of ultra-small platinum nanoparticles, Phys. Chem. Chem. Phys. 20 (2018) 5001–5011.
[28] G.L. Chen, X.J. Lin, J.N. Li, S.F. Huang, X. Cheng, Core-satellite ultra-small hybrid Ni@BT nanoparticles: a new route to enhanced energy storage capability of PVDF based nanocomposites, Appl. Surf. Sci. 513 (2020) 145877.
[29] L. Yang, Q.Y. Zhao, K.N. Chen, Y.Z. Ma, M.X. Shen, H.Y. He, H.J. Huang, H.L. Ji, Z.F. Wang, J.H. Qiu, Simultaneously realizing ultra-high energy density and discharge efficiency in PVDF composites loaded with highly aligned hollow MnO_2 microspheres, Compos. Part A 132 (2020) 105820.
[30] D.L. He, Y. Wang, S.L. Song, S. Liu, Y. Deng, Significantly enhanced dielectric performances and high thermal conductivity in poly(vinylidene fluoride)-based composites enabled by SiC@SiO_2 core-shell whiskers alignment, ACS Appl. Mater. Interfaces 9 (2017) 44839–44846.
[31] Y. Zhang, C.H. Zhang, Y. Feng, T.D. Zhang, Q.G. Chen, Q.G. Chi, L.Z. Liu, G.F. Li, Y. Cui, X. Wang, Z.M. Dang, Q.Q. Lei, Excellent energy storage performance and thermal property of polymer-based composite induced by multifunctional one-dimensional nanofibers oriented in-plane direction, Nano Energy 56 (2019) 138–150.
[32] H.X. Tang, Y.R. Lin, H.A. Sodano, Enhanced energy storage in nanocomposite capacitors through aligned PZT nanowires by uniaxial strain assembly, Adv. Energy Mater. 2 (2012) 469–476.
[33] J. Liu, Y. Luo, Y. Wang, Y. Deng, X.T. Xie, Bi_2S_3/poly(vinylidene fluoride) composite with high dielectric constant and unusual low dielectric loss based on preferentially oriented fillers, RSC Adv. 5 (2015) 96258–96264.
[34] L.M. Yao, S.F. Wu, Z.B. Pan, Y.P. Tan, F.P. Pi, R.K. Wang, J.W. Zhai, H.H.D. Chen, Enhancement of energy density in novel $Ba_{0.67}Sr_{0.33}TiO_3$ nanorod array nanocomposites, Mater. Des. 195 (2020) 109044.
[35] D. Zhang, W.W. Liu, R. Guo, K.C. Zhou, H. Luo, High discharge energy density at low electric field using an aligned titanium dioxide/lead zirconate titanate nanowire array, Adv. Sci. 5 (2018) 1700512.
[36] J.Y. Jiang, Z.H. Shen, J.F. Qian, Z.K. Dan, M.F. Guo, Y.H. Lin, C.W. Nan, L.Q. Chen, Y. Shen, Ultrahigh discharge efficiency in multilayered polymer nanocomposites of high energy density, Energy Storage Mater. 18 (2019) 213–221.
[37] F. Pedroli, A. Flocchini, A. Marrani, M.Q. Le, O. Sanseau, P.J. Cottinet, J.F. Capsal, Boosted energy-storage efficiency by controlling conduction loss of multilayered polymeric capacitors, Mater. Des. 192 (2020) 108712.
[38] Y.K. Zhu, Y.J. Zhu, X.Y. Huang, J. Chen, Q. Li, J.L. He, P.K. Jiang, High energy density polymer dielectrics interlayered by assembled boron nitride nanosheets, Adv. Energy Mater. 9 (2019) 1901826.
[39] J.Y. Jiang, Z.H. Shen, X.K. Cai, J.F. Qian, Z.K. Dan, Y.H. Lin, B.L. Liu, C.W. Nan, L.Q. Chen, Y. Shen, Polymer nanocomposites with interpenetrating gradient structure exhibiting ultrahigh discharge efficiency and energy density, Adv. Energy Mater. 9 (2019) 1803411.
[40] Y.Q. Chen, B.P. Lin, X.Q. Zhang, J.C. Wang, C.W. Lai, Y. Sun, Y.R. Liu, H. Yang, Enhanced dielectric properties of amino-modified-CNT/polyimide composite films with a sandwich structure, J. Mater. Chem. A 2 (2014) 14118–14126.
[41] Y.F. Wang, L.X. Wang, Q.B. Yuan, J. Chen, Y.J. Niu, X.W. Xu, Y.T. Cheng, B. Yao, Q. Wang, H. Wang, Ultrahigh energy density and greatly enhanced discharged efficiency of sandwich-structured polymer nanocomposites with optimized spatial organization, Nano Energy 44 (2018) 364–370.
[42] Q.G. Chi, Z.Y. Gao, C.H. Zhang, Y. Cui, J.F. Dong, X. Wang, Q.Q. Lei, Dielectric properties of sandwich-structured $BaTiO_3$/polyimide hybrid films, J. Mater. Sci. Mater. Electron. 28 (2017) 15142–15148.
[43] Y. Wang, Y.F. Hou, Y. Deng, Effects of interfaces between adjacent layers on breakdown strength and energy density in sandwich-structured polymer composites, Compos. Sci. Technol. 145 (2017) 71–77.
[44] M.A. Marwat, B. Xie, Y.W. Zhu, P.Y. Fan, W.G. Ma, H.M. Liu, M. Ashtar, J.Z. Xiao, D. Salamon, C. Samart, H.B. Zhang, Largely enhanced discharge energy density in linear polymer nanocomposites by designing a sandwich structure, Compos. Part A 121 (2019) 115–122.
[45] Q.G. Chi, Z.Y. Gao, T.D. Zhang, C.H. Zhang, Y. Zhang, Q.G. Chen, X. Wang, Q.Q. Lei, Excellent energy storage properties with high-temperature stability in sandwich-structured polyimide-based composite films, ACS Sustain. Chem. Eng. 7 (2019) 748–757.
[46] W.D. Sun, X.J. Lu, J.Y. Jiang, X. Zhang, P.H. Hu, M. Li, Y.H. Lin, C.W. Nan, Y. Shen, Dielectric and energy storage performances of polyimide/$BaTiO_3$ nanocomposites at elevated temperatures, J. Appl. Phys. 121 (2017) 244101.
[47] G.R. Chen, J.Q. Lin, X. Wang, W.L. Yang, D.P. Li, W.M. Ding, H.D. Li, Q.Q. Lei, Three-layer structure design for enhancing the energy efficiency and breakdown strength of $KTa_{0.5}Nb_{0.5}O_3$/polyimide nanocomposite films with high thermal stability, J. Mater. Sci. Mater. Electron. 28 (2017) 13861–13868.
[48] P.H. Hu, W.D. Sun, M.Z. Fan, J.F. Qian, J.Y. Jiang, Z.K. Dan, Y.H. Lin, C.W. Nan, M. Li, Y. Shen, Large energy density at high-temperature and excellent thermal stability in polyimide nanocomposite contained with small loading of $BaTiO_3$ nanofibers, Appl. Surf. Sci. 458 (2018) 743–750.
[49] Q.G. Chi, B. Wang, T.D. Zhang, C.H. Zhang, Y.Q. Zhang, X. Wang, Q.Q. Lei, Designing of surface modification and sandwich structure: effective routs to improve energy storage property in polyimide-based composite films, J. Mater. Sci. Mater. Electron. 30 (2019) 19956–19965.
[50] Q.G. Chi, Z.Y. Gao, C.H. Zhang, T.D. Zhang, Y. Cui, X. Wang, Q.Q. Lei, Microstructures and energy storage property of sandwiched BZT-BCT@Fe_3O_4/polyimide composites, J. Mater. Sci. Mater. Electron. 30 (2019) 1–8.
[51] J.S. Ru, D.M. Min, M. Lanagan, S.T. Li, G. Chen, Energy storage properties of polyimide/$BaTiO_3$ nanocomposite films and their breakdown mechanism in a wide content range, Appl. Phys. Lett. 115 (2019) 213901.
[52] T. Nishino, M. Kotera, N. Inayoshi, N. Miki, K. Nakamae, Residual stress and microstructures of aromatic polyimide with different imidization processes, Polymer 41 (2000) 6913–6918.
[53] J.L. Pan, K. Li, S. Chuayprakong, T. Hsu, Q. Wang, High-temperature poly (phthalazinone ether ketone) thin films for dielectric energy storage, ACS Appl. Mater. Interfaces 2 (2010) 1286–1289.
[54] Y. Thakur, T. Zhang, C. Iacob, T.N. Yang, J. Bernholc, L.Q. Chen, J. Runt, Q.M. Zhang, Enhancement of the dielectric response in polymer nanocomposites with low dielectric constant fillers, Nanoscale 9 (2017) 10992–10997.
[55] S.T. Li, G.L. Yin, G. Chen, J.Y. Li, S.N. Bai, L.S. Zhong, Y.X. Zhang, Q.Q. Lei, Short-term breakdown and long-term failure in nanodielectrics: a review, IEEE Trans. Dielectr. Electr. Insul. 17 (2010) 1523–1535.
[56] D.M. Min, C.Y. Yan, R. Mi, C. Ma, Y. Huang, S.T. Li, Q.Z. Wu, Z.L. Xing, Carrier transport and molecular displacement modulated dc electrical breakdown of polypropylene nanocomposites, Polymers 10 (2018) 1207.